Scientia Iranica B (2022) 29(4), 1782–1794

SCIENTIA IRANICA

Sharif University of Technology
Scientia Iranica
Transactions B: Mechanical Engineering
http://scientiairanica.sharif.edu

Evaluation of the thermo-fluid performance of a split-winglet supported elliptical tube type fin-and-tube heat transfer surface

S.K. Sarangi and D.P. Mishra*

Birla Institute of Technology, Mesra, Ranchi, Jharkhand, 835215, India.

Received 5 August 2020; received in revised form 29 September 2021; accepted 29 November 2021

KEYWORDS
Fin-and-tube heat exchanger;
Split winglet pair;
Rectangular winglets;
Elliptical tubes;
Stream wise location;
Span wise location;
Angle of attack.

Abstract. The main objective of the current study is to investigate the vortex generator supporting fin-tube heat transfer surface equipped with inline elliptical tubes by performing numerical simulations governed by finite volume method. It also aims at minimizing air-side thermal resistance using rectangular winglet pairs. Then, the thermo-fluid performance of the baseline model was evaluated for the circular and elliptical tube configurations. According to the findings, while the former increased the heat transfer, the latter decreased the pressure drop. The effect of the span- and stream-wise separation of the split winglet pair and attack angle on the heat transfer and pressure drop performance was also examined in detail, the results of which were presented in the forms of Nu, f, and η. The optimum stream- and span-wise locations for the front and rear winglet pairs were identified based on highest enhancement factor. It was also found that the optimum attack angle of the front and rear winglet pairs was different for the maximum enhancement factor.

1. Introduction

Fin-and-Tube Heat Exchangers (FTHXs) are categorized into the gas-liquid types of heat exchangers that are used in air-conditioning and refrigeration systems, automobile and petrochemical industries, and electronic chip cooling. Usually, the liquid-side thermal resistance and fin-side conductive resistance in FTHXs are quite low due to the high heat transfer coefficient of the liquid flowing inside the tube and high thermal conductivity of the fin material, respectively. However, the heat transfer coefficient of air is very low due to its thermo-physical properties; therefore, the air-side thermal resistance has a greater share in the overall thermal resistance. Moreover, in such heat exchangers, thermal mixing is poor in the wake region behind the tubes. In this regard, to improve the performance of the heat exchanger against these thermal and geometrical constraints, several heat transfer enhancement techniques should be employed.

Passive heat transfer enhancement methods are more common in practice since the only power required during their operation is for pumping the fluid across the heat exchanger to compensate for the pressure drop. The winglet-type Vortex Generator (VG) is a passive heat transfer enhancement tool with the potential to introduce the secondary flow vortices, and it intensifies the hot and cold fluid mixing near the wake region. They also delay the flow separation and modify the thermal boundary layer. Both heat transfer and pressure drop performance of the heat exchanger depend on the winglet configuration and location.

In order to enhance the heat transfer contribution

*. *Corresponding author. Tel.: +91-7250582643*
E-mail address: diptimishraster@gmail.com (D.P. Mishra)

doi: 10.24200/sci.2021.56552.4784

of the air side, many researchers have attempted to modify the fin geometry and installation of VGs over the fin surface. However, changes in the fin configuration have resulted in higher pressure drop and slight improvement in the heat transfer [1]. The installation of winglets as VGs over the fin surface intensifies the heat transfer coefficient and, consequently, results in significant enhancement in the heat transfer. Further, two winglet orientations have drawn considerable attention from many researchers in the open literature. For instance, Biswas et al. [2], Torii et al. [3], and Jain et al. [4] used the "common-flow-up" winglet orientations which effectively compressed the wake region and accelerated the flow near the wake region. Vasudevan et al. [5], Sohankar and Davidson [6], and Kwak et al. [7] used the "common-flow-down" winglet orientation in their studies where high-momentum fluid was introduced in the tube wake region to improve the thermal mixing [8].

A few authors have also investigated the inline and staggered orientation of the winglets. For instance, Joardar and Jacobi [9,10] evaluated the impact of inline (alternate tubes) and staggered (consecutive tubes) placement of delta winglet VGs. They found that in order to achieve the same heat transfer enhancement, the staggered winglet configuration caused relatively lower pressure drop. Similarly, based on their numerical study, He et al. [11] reported that compared to the inline arrangement, the staggered arrangement of VGs caused almost the same heat transfer effect, but with reduced pressure drop.

Many authors have considered optimization techniques in the open literature to solve multi-objective problems. For instance, Richter do Nascimento et al. [12] used Computational Fluid Dynamics (CFD) techniques and genetic algorithms to improve the design capabilities in a plate-fin heat exchanger with offset strip-fins. They reported a reduction in the pressure drop of 55.4% and 72.3%, respectively, on the hot and cold sides. Strategic selection of the population size can help a multi-objective genetic algorithm to balance the convergence time and the accuracy of the results. Galuzio et al. [13] proposed a new python-based software product called Bayesian optimization software capable of determining better quality Pareto front approximations with minimum evaluations of the objectives. The owl optimization algorithm [14] applied to the shell and tube heat exchangers resulted in significant enhancement in the performance of both single- and multi-objective optimization. Lemouedda et al. [15] employed optimization techniques based on Pareto optimal strategy and proposed optimum sets of attack angle for Reynolds number ranging from 200 to 1200. They compared the inline and staggered positioning of tube rows and reported that the latter had more heat transfer effect in the considered range of Re. Similarly, Salviano et al. [16] performed a SIMPLEX method-based optimization study for FTHX and highlighted the advantages of enhancement in the heat transfer of the staggered tube rows over inline tubes. For a given design space, the SIMPLEX method provides the simplest possible polytope that can be used in optimization studies on non-linear problems.

Venegas et al. [17] presented a critical review of desiccant-coated heat exchangers and suggested possible development in terms of enhancement in the energy and dehumidification performance of the system. Wajs et al. [18] performed several simulations for a mini-channel heat exchanger to determine the flow rate and pressure field distribution along with the temperature distribution in the solid and fluid zones. Tian et al. [19] compared the performance of both delta and rectangular VGs and found that the former exhibited better overall performance while the latter delivered better heat transfer effect.

Saha et al. [20] also carried out a synergy-based study to compare the rectangular and delta VGs arranged in both "common-flow-up" and "common-flow-down" orientations. They reported more heat transfer enhancement in the case of rectangular winglet pairs than that of their counterparts. Sinha et al. [21] examined different possible winglet arrangements with "common-flow-up" and "common-flow-down" orientations. They remarked that the "common-flow-up" orientation in series resulted in greater heat transfer performance. Gentry and Jacobi [22,23] conducted experiments using the naphthalene sublimation technique to study the impact of delta winglet VG in a flat-plate flow.

In recent years, many investigators have focused on determining the optimum winglet locations in FTHX. For instance, Pesteei et al. [24] experimentally examined five different locations of delta winglet pair around a single tube and determined the optimum locations in the tube centre. Arora et al. [25] performed a similar type of investigation with three rows of inline tubes and twenty possible locations of VGs. Sarangi and Mishra [26] and Sarangi et al. [27] did some numerical simulations with rectangular VGs in a FTHX and determined the optimum winglet number, winglet attack angle, and winglet locations (stream-wise and span-wise). They also examined the impact of wavy nature of the rectangular winglets in the FTHX [28]. Naik and Tiwari [29] took into account the "common-flow-down" oriented VGs in their study and examined the impacts of the attack angle, Re, and stream- and span-wise locations of the VGs.

A review of the available literature revealed that the VGs had the potential to effectively enhance the performance of the heat transfer using mechanisms such as delaying flow separation, modification of the boundary layer, and vortex generation. The rectangular winglet pairs were found to be more efficient in heat transfer augmentation than the delta winglet pairs [19,20]; however, they had a major drawback, i.e., relatively higher pressure drop. The present study aims to minimize the pressure drop associated with the application of rectangular winglet pairs. To this end, the VGs were positioned with a heretofore-unused combination, i.e., split winglet pairs over the elliptical tubes, to enhance the performance of heat transfer with lower pressure drop penalty. The full-length winglet used in the previous studies [27] was divided into equal parts in the present study, and their optimum locations were assessed to guarantee greater control over thermal mixing behind the tubes.

Compared to the circular tubes, the elliptical tube shape causes relatively less pressure drop due to its aerodynamic shape [30]. For this reason, the present analysis took into account this advantage of the elliptical tubes as well as their overall performance in comparison to the conventional circular tube FTHX examined under the same surface area condition. It is expected that the split winglet pairs together with the elliptical tubes can significantly enhance the thermo-fluid performance of the FTHXs.

2. Mathematical formulation

2.1. Physical and computational model

Figure 1 shows the split-winglet-supported FTHX characterized by five rows of tubes along the stream and four rows of tubes transverse to the stream. The basic geometry (baseline model) concept of the considered FTHX was borrowed from the study of Joardar and Jacobi [9,10]. The split winglet pairs were symmetrically positioned around the elliptical tubes, as depicted in Figure 2. According to this figure, the total winglet length ($L_1 + L_2$) is 10.67 mm which is equal to the circular tube diameter. In addition, the fin spacing and channel length along the stream are measured as 3.63 mm and 127 mm, respectively. The pitch for the tube is 25.4 mm, and the VGs with "common-flow-up" configuration are placed at suitable attack angles. The surface area of the elliptical tube (a = 4 mm, b = 6.52 mm) is kept at the same value as that of the circular tube. Due to the symmetric orientation of the tubes and winglets, the region shown within the indicated region in Figure 1 is chosen as the computational domain.

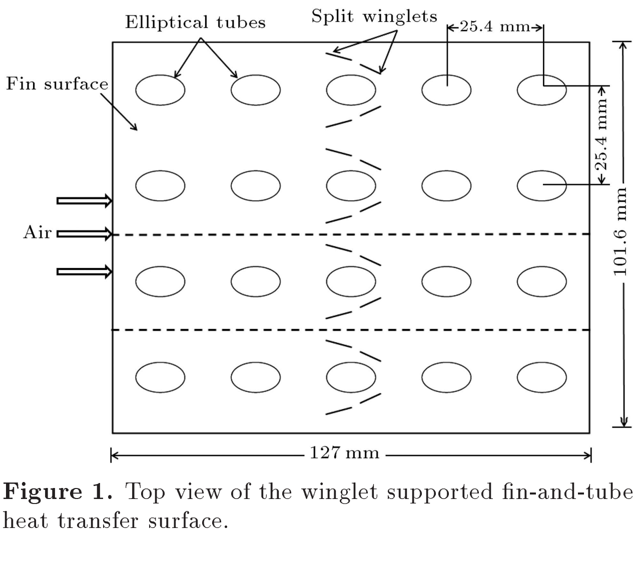

Figure 1. Top view of the winglet supported fin-and-tube heat transfer surface.

2.2. Governing equations

To simplify the modeling of the heat transfer process for the FTHX, some assumptions were made. For instance, the flow is assumed to be steady, laminar, and incompressible. In addition, the working fluid is air and its density varies with changes in the temperature governed by the ideal gas equation. The following Navier-Stokes equations are applicable to the considered flow model:

Continuity equation:

$$\frac{\partial}{\partial x_i}(\rho u_i) = 0, \tag{1}$$

Momentum equation:

$$\frac{\partial}{\partial x_i}(\rho u_i u_k) = \frac{\partial}{\partial x_i}\left(\mu \frac{\partial u_k}{\partial x_i}\right) - \frac{\partial p}{\partial x_k}. \tag{2}$$

In the operating temperature range, the dynamic viscosity, μ, is assumed to be constant.

Energy equation:

$$\frac{\partial}{\partial x_i}(\rho u_i T) = \frac{\partial}{\partial x_i}\left(\frac{k_a}{C_p}\frac{\partial T}{\partial x_i}\right). \tag{3}$$

Conduction equation is solved to obtain the temperature distribution on the winglets and fin surfaces, as shown below:

Conduction equation:

$$\frac{\partial^2 T}{\partial x_i^2} = 0. \tag{4}$$

2.3. Boundary conditions

Figure 3(a) and (b) describe the boundary condition applied to the surfaces of the computational domain. The inlet boundary was imposed based on the velocity inlet condition of $U_{in} = 2 - 3.3$ m/s corresponding to $Re_H = 500 - 819$ at a uniform temperature of 310.6 K. Symmetry condition was applied to the upper, lower, and side boundaries. Pressure outlet condition was also applied to the outlet surface. The cold tube walls were then considered under no-slip and constant

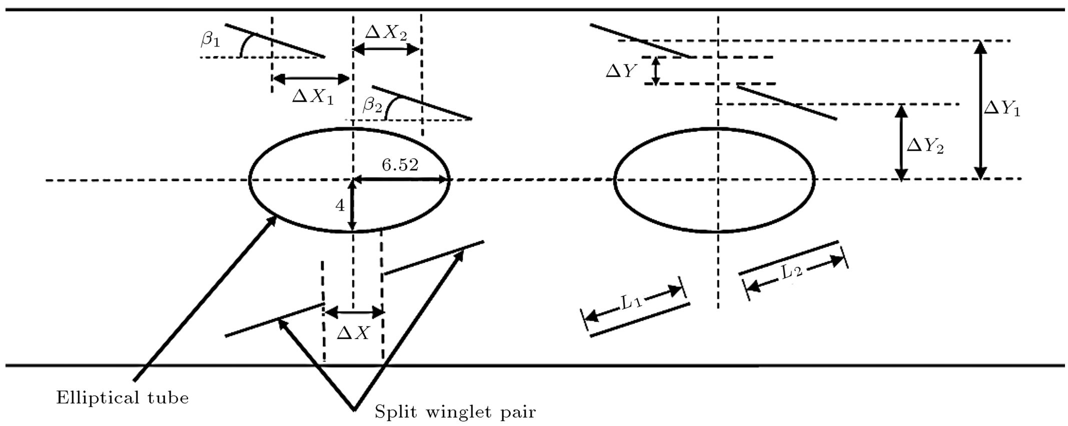

Figure 2. Top view of split winglet orientation around elliptical tubes.

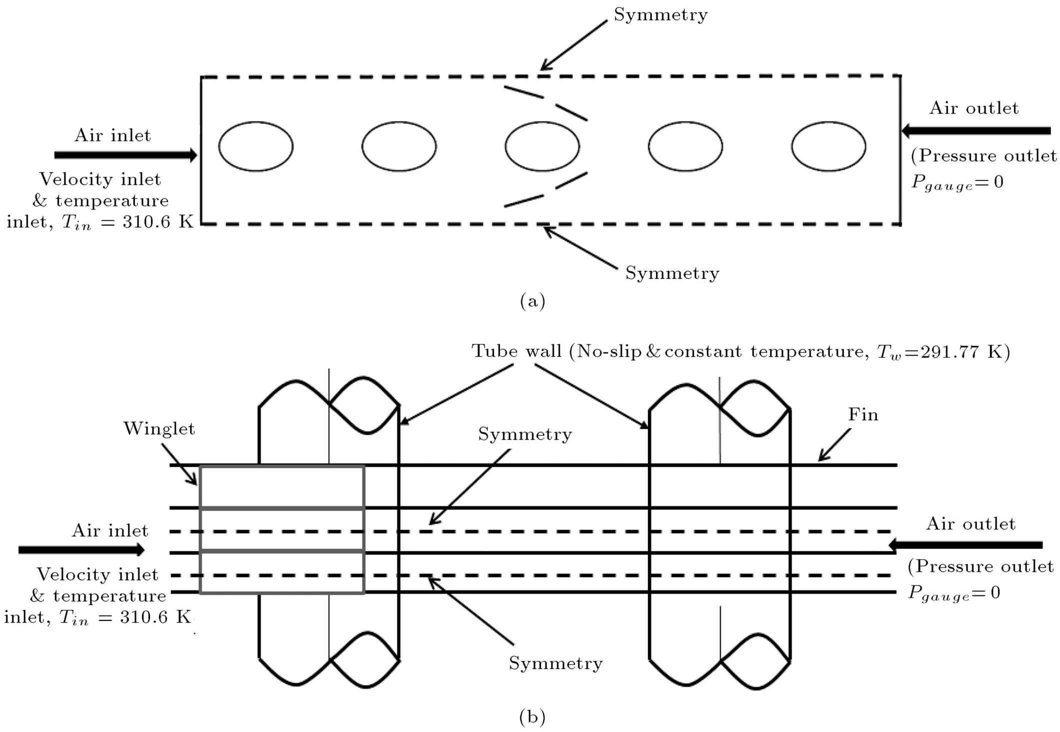

Figure 3. (a) Top view and (b) side view (shown for third and fourth tubes only) of the computational domain with applied boundary conditions.

temperature condition (T_w = 291.77 K) and also, with the assumptions that the tube wall material is aluminum bearing high thermal conductivity and that the liquid inside the tubes has a high convective heat transfer coefficient.

2.4. Computation of performance parameters

The performance parameters are defined as [30]:

Overall heat transfer:

$$Q = \dot{m}c_p(\overline{T_o} - \overline{T}_{in}), \tag{5}$$

$$LMTD, \qquad \Delta T = \frac{(T_w - \bar{T}_{in}) - (T_w - \bar{T}_o)}{\ln[(T_w - \bar{T}_{in})/(T_w - \bar{T}_o)]}, \tag{6}$$

Reynolds number:

$$Re_H = \frac{\rho u_{in}}{\mu} H, \tag{7}$$

Nusselt number:

$$Nu = \frac{hH}{k_a}, \tag{8}$$

Heat transfer coefficient:

$$h = \frac{Q}{A_T . \Delta T}. \tag{9}$$

Friction factor can be obtained as defined by Nascimento et al. [31]:

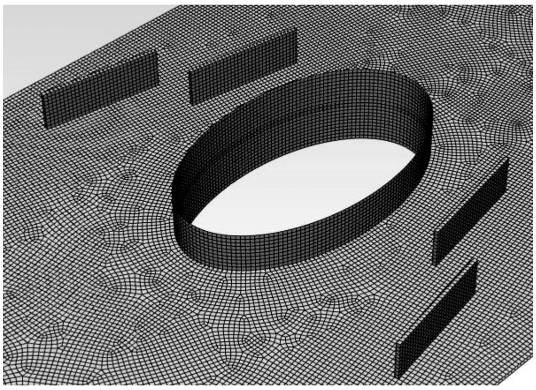

Figure 4. Cut section view of meshes around the split winglet pair and elliptical tube.

$$f=\frac{\Delta p}{\frac{\rho u_{in}^2}{2}\frac{L}{H}},\qquad(10)$$

Enhancement factor [27,32]:

$$\eta=\left(\frac{Nu}{Nu_0}\right)\left(\frac{f}{f_0}\right)^{-1/3}.\qquad(11)$$

2.5. Numerical method

Finite volume method-based three-dimensional numerical simulations were performed using Fluent 17 multi-grid solver for thermo-fluid analysis of the considered FTHX. Semi-Implicit Method for Pressure Linked Equation (SIMPLE) algorithm was employed to couple the velocity and pressure. The entire flow domain consists of solid (fins, tubes, and winglets) and fluid zones which are meshed with structured hexahedral elements. Figure 4 shows the generated grid system.

The convective terms in the governing equations are discretized by the second-order upwind scheme resulting in the improvement of about 0.5% over the first-order upwind scheme. The tolerance for convergence was set as 10^{-6} for energy and 10^{-3} for continuity and momentum.

3. Results and discussion

3.1. Grid test and validation of numerical results

A grid assessment test is required prior to performing numerical solutions to ensure the best mesh size with regard to computational accuracy. The grid test shown in Table 1 was conducted for both circular and elliptical tube types of FTHXs.

The grid test covered a wide range of grid sizes from a coarse grid number of about 700,000 to a very fine grid size of about 1,900,000. The Nusselt number obtained against each grid number for the circular and elliptical tube configurations increases continuously as the mesh is refined to a finer size. However, the change in the Nusselt number beyond the grid number of about 1,800,000 is almost negligible, thus indicating grid independence from the solution. In this respect, the present numerical study used the cell size corresponding to the grid number of about 1,800,000 for generating the grids. Similar grid tests were also conducted on the VG supported FTHX models.

Table 1. Nusselt number variation with grid number for circular and elliptical tube FTHX models.

Grid number	Nu_c	Grid number	Nu_e
724,564	3.95	694,013	3.68
1,013,264	4.37	1,071,079	3.92
1,354,184	4.72	1,385,641	4.39
1,548,366	4.79	1,680,520	4.45
1,789,494	4.81	1,809,150	4.47
1,927,784	4.82	1,971,680	4.48

The results obtained from CFD for the baseline model were validated through the experimental results [10,33] to prove the reliability and the accuracy of the numerical model. Table 2 presents more details of the experimental models [10,33]. As observed in Figure 5(a) and (b), the present simulated results of h and Δp, respectively, agreed well with the experimental results obtained by Joardar and Jacobi [10] with the maximum deviation of less than 10%. The uncertainty reported in the experimental results varied from $\pm 4\%$ to $\pm 15\%$ for h and Δp, respectively. Similarly, Figure 5(c) presents a comparison of the Nu obtained from the present CFD and the results obtained from the experiments conducted by Kays and London [33]. The maximum deviation of the CFD results from the experiment lies within 7% with a reported uncertainty of $\pm 5\%$. In summary, the numerical model exhibits good agreement with the experimental results [10,33], hence being reliable in terms of predicting the performance of the FTHX.

3.2. Heat transfer and pressure drop assessment of plain FTHX with circular and elliptical tube geometries

In this section, the performance of smooth FTHX is evaluated considering the circular and elliptical tube geometries separately. For the ideal comparison of the performance of the two tube geometries, their surface area was assumed to be the same in terms of size. Given that the two tube geometries result in different hydraulic diameters, the fin spacing was selected as the standard characteristic dimension for the calculation of Re_H.

Figure 6 shows the variations of Nu for circular and elliptical tube configurations against Re_H ranging from 500 to 800. According to the illustrated plot, the heat transfer performance is marginally high for the circular tube at low Re_H which increases substantially

Table 2. Details of the FTHX model used for validation of the numerical model.

Parameter	Kays and London [33]	Joardar and Jacobi [10]
D	10.2 mm	10.67 mm
P_t	22 mm	25.4 mm
P_l	25.4 mm	25.4 mm
n	3	7
H	3.2 mm	3.63 mm
F_t	0.33 mm	0.18 mm
T_w	300 K	291.77 K
T_{in}	340 K	310.6 K
U_{in}	$1.3 - 2.6$ m/s	$0.5 - 9.5$ m/s

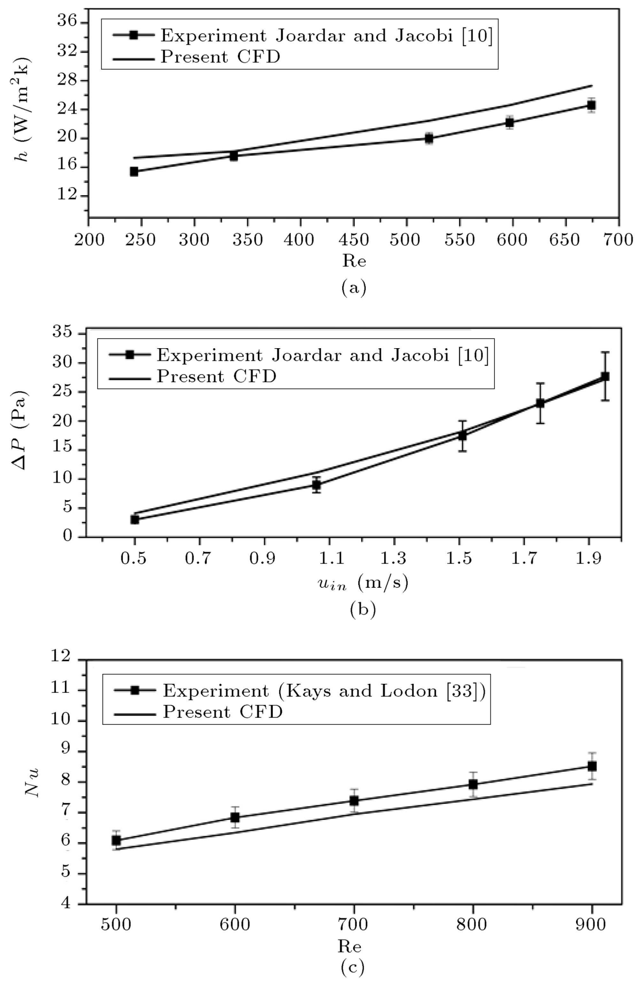

Figure 5. Comparison of CFD results with the baseline model of (a) and (b) experimental results for baseline case of Joardar and Jacobi [10], and (c) baseline model experimental results of Kays and London [33].

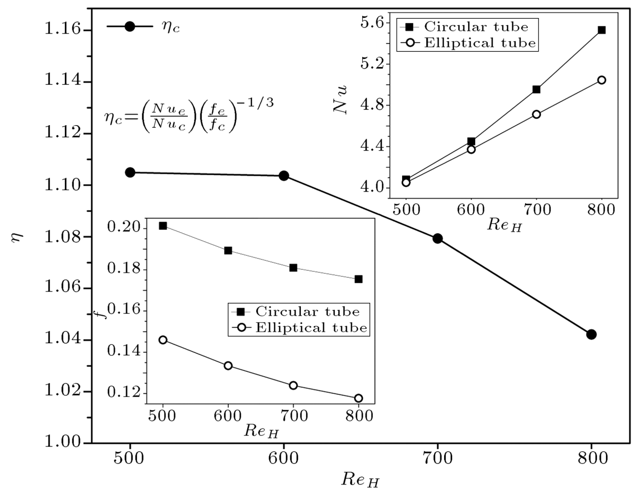

Figure 6. Heat transfer and fluid flow parameters for circular and elliptical tube geometries.

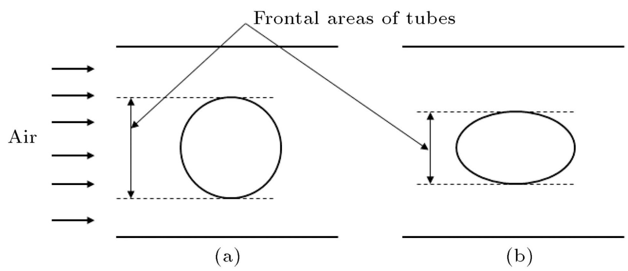

Figure 7. Top view of the considered tube geometries: (a) Circular tube and (b) elliptical tube.

when the Re_H increases up to more than 700. Figure 7 confirms that the circular tube has a larger frontal area than the elliptical tube and with a rise in Re_H, the heat transfer rate increases due to the higher local convective heat transfer coefficient. However, compared to the elliptical tube, circular tube has a larger frontal area which results in a substantial increase in the form drag and pressure drop. As shown in Figure 6, the elliptical tube geometry has two main advantages of relatively lower pressure drop and friction factor due to its aerodynamic shape. This figure also suggests an enhancement factor based on the circular tube geometry (η_c) for the elliptical tube geometry. Due to low pressure drop of the elliptical tube, its thermo-fluid performance is higher than that of the circular tube type FTHX.

3.3. Effect of span wise variation of split winglets pairs

This section examines the effect of span-wise variations of the split winglet pairs on the performance of FTHX based on the numerical simulations. The two winglet pairs with a length of 5.335 mm each were symmetrically placed around the elliptical tube at a constant attack angle of 10°. The stream-wise center distances of the first and second winglets are defined as $\Delta X_1 = -2.67$ mm and $\Delta X_2 = +2.67$ mm, respectively. The negative sign is indicative of the upstream placement of the VG relative to the tube center, while the positive sign shows the downstream position of the VG pair. In addition, while the first winglet pair was moved away from the tube, the second winglet pair was brought close to the tube, both with an interval of 0.5 mm.

The Nusselt number plot in Figure 8 shows the variations in the heat transfer performance of the FTHX with the span-wise distance of VGs. The first and second winglet pairs were initially placed at $\Delta Y_1 = 8.5$ mm and $\Delta Y_2 = 7.5$ mm, respectively. In this location, the split winglet pair practically acts like a full-length winglet (Figure 9(a)), which drives the fluid near to the wake region and enhances the local heat transfer coefficient. If $\Delta Y_1 = 9$ mm and $\Delta Y_2 = 7$ mm (Figure 9(b)), a small gap is created between the split winglets and a majority of the fluid is driven towards the adjacent tube by rear winglet pair of split winglets which compresses the thermal isolated zone and increases both heat transfer and pressure drop. As the value of ΔY_1 further increases to 9.5 mm, more fluid is driven towards the downstream tubes. However, when the value of ΔY_2 reaches closely 6.5 mm, the gap between the split winglets will increase further and the majority of the fluid will pass through the gap without coming close to the tube wake region (Figure 9(c)).

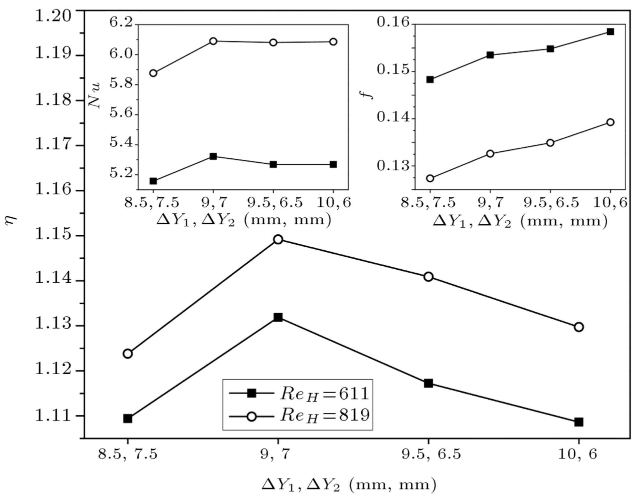

Figure 8. Nusselt number, Friction factor, and enhancement factor as a function of winglet pair's span-wise position.

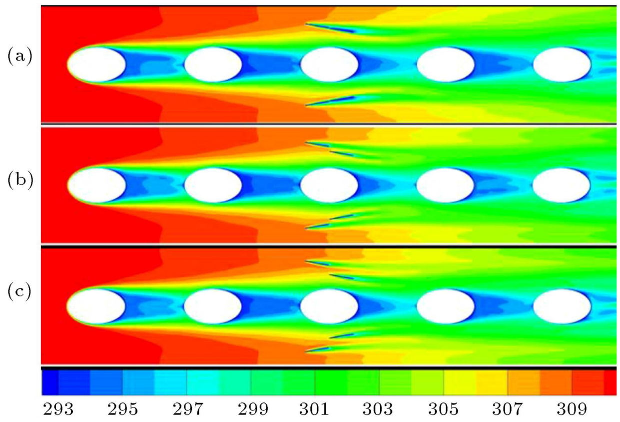

Figure 9. Temperature contours (unit: K) over the fin surface for: (a) $\Delta Y_1 = 8.5$ mm, $\Delta Y_2 = 7.5$ mm, (b) $\Delta Y_1 = 9$ mm, $\Delta X_2 = 7$ mm, and (c) $\Delta Y_1 = 9.5$ mm, $\Delta Y_2 = 6.5$ mm.

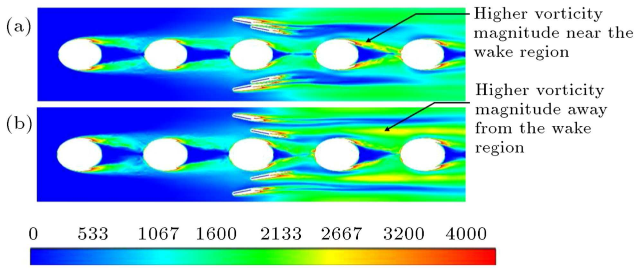

Figure 10. Vorticity magnitude (unit: s^{-1}) contours over the fin surface for (a) $\Delta Y_1 = 9$ mm, $\Delta X_2 = 7$ mm and (b) $\Delta Y_1 = 10$ mm, $\Delta Y_2 = 6$ mm.

As a result, the heat transfer performance is slightly degraded. However, as more fluid is constrained to move within the gap between the split winglet pairs, the pressure drop rises continuously, as shown in the plot of friction factor in Figure 8.

In order to enhance the heat transfer, the low-temperature fluid behind the tubes and relatively high-temperature fluid in the mainstream flow are mixed together. According to the vorticity contours in Figure 10, the vorticity magnitude is greater near the wake region of the adjacent tube for $\Delta Y_1 = 9$ mm and $\Delta Y_2 = 7$ mm. The high vorticity magnitude indicates stronger secondary flow intensity which promotes the effective heat exchange between the cold fluid behind the tubes and mainstream flow, hence more heat transfer enhancement.

Enhancement factor in Figure 8 exhibits the overall effect of the variations in the span-wise placement of the split winglet pair. The enhancement factor reaches its maximum value at locations $\Delta Y_1 = 9$ mm and $\Delta Y_2 = 7$ mm, and then it falls continuously. An increase in the Nusselt number is not significant beyond $\Delta Y_1 = 9$ mm and $\Delta Y_2 = 7$ mm; however, the pressure drop penalty increases substantially, indicating that beyond these span-wise locations, the enhancement in the pressure drop is larger than that in the heat transfer as a result of which the enhancement factor drops continuously.

3.4. Effect of stream-wise variation of split winglets pairs

The effect of the stream-wise locations of the split winglet pair on the performance of the FTHX was examined through numerical simulations. The two VG pairs were symmetrically placed on the elliptical tubes at a constant attack angle of 10°. The first and second winglets were placed at their optimum span-wise locations of $\Delta Y_1 = 9$ mm and $\Delta Y_2 = 7$ mm, respectively. The first and second winglet pairs were then simultaneously pushed towards the upstream and downstream of the tube, respectively, with a constant step size of 0.5 mm. The negative sign shows the distance measured upstream of the tube, while the positive sign shows the distance measured downstream of the tube.

Figure 11(a) shows the variations in the Nu with the stream-wise distance of the split winglet pairs. First, the first and second winglet pairs were placed at the stream-wise locations of $\Delta X_1 = -2.67$ mm and $\Delta X_2 = +2.67$ mm, respectively. With an increase in the stream-wise eccentric separation (ΔX) between the split winglet pairs, the heat transfer performance degrades continuously.

A comparison of the temperature contours from Figure 12(a) and (b) reveals that the temperature in the wake zone is higher when there is no stream-wise eccentric separation ($\Delta X_1 = -2.67$ mm, $\Delta X_2 = +2.67$ mm) between the two split winglet pairs, and the

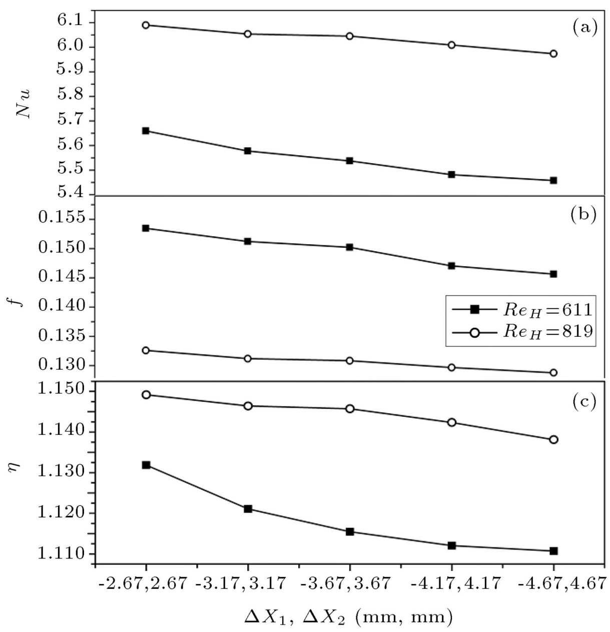

Figure 11. Thermo-fluid performance parameters as a function of stream-wise locations of split winglet pairs.

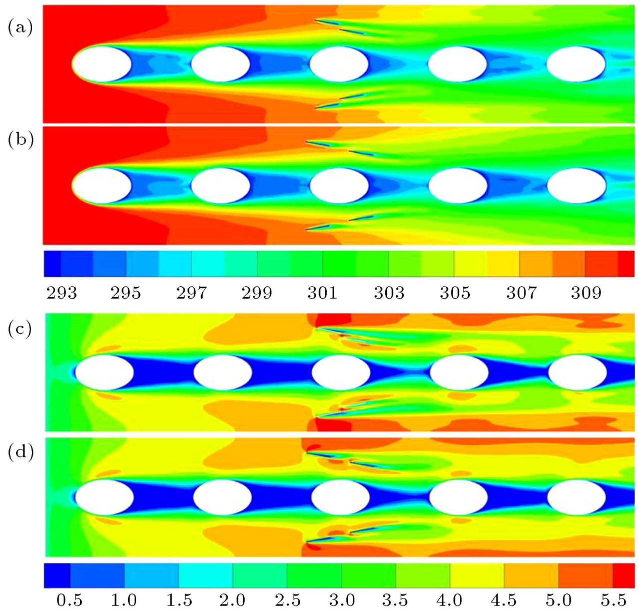

Figure 12. Temperature contours (unit: K) over the fin surface for (a) $\Delta X_1 = -2.67$ mm, $\Delta X_2 = +2.67$ mm and (b) $\Delta X_1 = -4.17$ mm, $\Delta X_2 = +4.17$ mm. Velocity contours over the fin surface for (c) $\Delta X_1 = -2.67$ mm, $\Delta X_2 = +2.67$ mm and (d) $\Delta X_1 = -4.17$ mm, $\Delta X_2 = +4.17$ mm.

gap between the winglets is only caused by the span-wise eccentric separation. Since the gap is narrow, a negligible amount of the fluid is constrained to move within the gap and a great portion of the fluid is driven towards the wake region. As a result, both Nu and f values remain high for the present configuration.

When the second winglet pair advances downstream, it does not form the converging region with the tube surface, thus making the flow impinge with a relatively low velocity, while the majority of the fluid passes through the gap between the split winglet pairs. This results in relatively low thermal mixing and heat transfer performance (Figure 11(a)) with less pressure drop (Figure 11 (b)). In addition, a comparison of the velocity contours in Figure 12(c) and (d) shows that the absence of stream-wise eccentric separation between the winglets ($\Delta X = 0$ mm) would lead to greater compression of the winglet supported tube as well as the adjacent tube. Thus, the winglet locations of $\Delta X_1 = -2.67$ mm and $\Delta X_2 = +2.67$ mm ensure maximum heat transfer performance.

Figure 11(c) presents an enhancement factor to summarize the overall effect of stream-wise location of the split winglet pairs on the performance of the FTHX. The enhancement factor reaches its maximum value at the stream-wise locations of $\Delta X_1 = -2.67$ mm and $\Delta X_2 = +2.67$ mm ($\Delta X = 0$ mm) and gradually decreases upon increasing the stream-wise eccentric separation, i.e., $\Delta X = 1$ mm, 2 mm, and 3 mm, between the two winglet pairs. For all the other considered stream-wise locations of the split winglet pairs, both Nu and f decrease continuously. On the contrary, the continuous reduction in the enhancement factor indicates that the decrease in the heat transfer is more dominant than that in the pressure drop in the case of increased stream-wise eccentric separation ($\Delta X = 1$ mm, 2 mm, 3mm).

3.5. Effect of variation in attack angle of the split winglet pair

The impact of the attack angle of the split winglet pair on the performance of the FTHX was examined based on the numerical simulation results. The attack angle of each winglet pair varies from 5° to 20° with a step size of 5°. A total of 16 possible combinations of attack angles for the two winglet pairs (β_1 and β_2) were examined, the results of which are presented in Table 3. The length of the first and second winglet pairs was considered to be 5.335 mm. The split winglet pairs were placed at their optimum stream- and span-wise locations corresponding to $\Delta X_1 = -2.67$ mm, $\Delta Y_1 = 9$ mm, $\Delta X_2 = +2.67$ mm, and $\Delta Y_2 = 7$ mm.

Table 3 shows the variations in Nu, f, and η as the functions of the first and second attack angles (β_1 and β_2) of the split winglet pairs for both $Re_H = 611$ and $Re_H = 819$. According to this table, the value of Nu is always higher when the attack angle of the first winglet pair (β_1) is greater than that of the second winglet pair (β_2). These two winglet pairs contribute differently to the overall heat transfer performance. The first winglet pair pushes the incoming flow towards the constricted section created between the second winglet pair and tube as well as towards the downstream side through the span-wise eccentric gap created between the two winglet pairs. The second winglet pair placed relatively closer to the tube, however, is responsible only for minimization of the wake zone of the VG supported tube, as illustrated in Figure 13(a) and (b).

In case the attack angle of the first winglet pair is kept larger than that of the second winglet pair, as depicted in Figure 13(c), the wake regions of the VG-supported tube and adjacent tubes are effectively

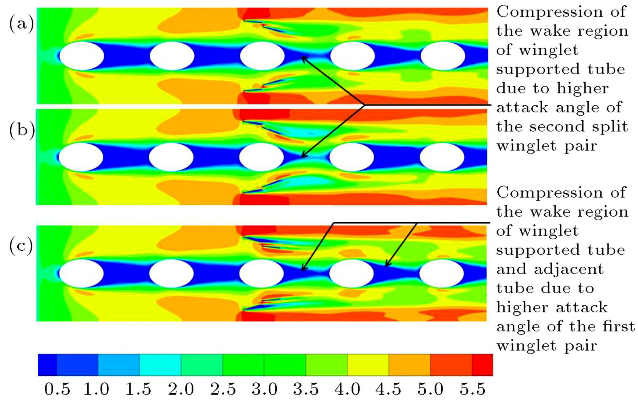

Figure 13. Velocity contours (unit: m/s) over the fin surface for (a) $\beta_1 = 5°$, $\beta_2 = 15°$, (b) $\beta_1 = 10°$, $\beta_2 = 20°$, and (c) $\beta_1 = 15°$, $\beta_2 = 5°$.

Table 3. Performance parameters variation with attack angle of the split winglet pairs.

$\boldsymbol{\beta_1}$, $\boldsymbol{\beta_2}$	$\boldsymbol{Re_H = 611}$			$\boldsymbol{Re_H = 819}$		
	$\boldsymbol{Nu}$	$\boldsymbol{f}$	$\boldsymbol{\eta}$	$\boldsymbol{Nu}$	$\boldsymbol{f}$	boldmath η
5, 5	5.37	0.1443	1.096	5.88	0.1240	1.136
5, 10	5.56	0.1443	1.136	5.99	0.1274	1.146
5, 15	5.54	0.1518	1.113	6.00	0.1320	1.134
5, 20	5.52	0.1584	1.093	5.89	0.1363	1.102
10, 5	5.61	0.1487	1.136	6.07	0.1287	1.157
10, 10	5.66	0.1535	1.132	6.09	0.1326	1.149
10, 15	5.64	0.1606	1.115	6.05	0.1384	1.126
10, 20	5.55	0.1658	1.083	5.97	0.1457	1.092
15, 5	**5.80**	**0.1576**	**1.150**	**6.22**	**0.1370**	**1.162**
15, 10	5.82	0.1654	1.136	6.25	0.1430	1.151
15, 15	5.67	0.1688	1.099	6.19	0.1534	1.112
15, 20	5.66	0.1773	1.079	6.13	0.1607	1.085
20, 5	5.76	0.1704	1.114	6.33	0.1497	1.148
20, 10	5.75	0.1775	1.095	6.32	0.1581	1.126
20, 15	5.76	0.1865	1.081	6.15	0.1676	1.073
20, 20	5.74	0.1917	1.066	6.23	0.1734	1.076

Table 4. Comparison of the maximum overall enhancement obtained with the proposed split winglet configuration with recent contributions from different researchers.

Researches	Surface modification	Flow condition	($\eta_{\max}$)
Present work	Split Rectangular winglet pairs	Re_H= 500-819	16.2%
Naik and Tiwari [29]	Rectangular winglets	Re_D= 2000-4000	10%
Gholami et al. [34]	Wavy rectangular winglets	Re_{Dh}= 400-800	7.4%
Gholami et al. [35]	Corrugated fins	Re_{Dh}= 200-900	16%
Qian et al. [36]	Rectangular winglets	Re_{Dh}= 1300-2000	11%
Naik and Tiwari [37]	Rectangular winglets	Re_D= 2000-10000	10%
Modi et al. [38]	Rectangular winglets with holes	Re_{Dh}= 400-2000	16.5%
Khan and Li [39]	Rectangular and delta winglet	Re_{Dh}= 380-1140	14.4%

compressed compared to the earlier cases (Figure 13(a) and (b)), thus resulting in enhanced thermal mixing and heat transfer performance. According to Table 3, upon increasing the attack angle of either the first or second VG pair, the exposed area of the winglet would increase, hence greater resistance to the incoming flow. Consequently, the pressure drop increases substantially across the flow domain.

Table 3 also lists the enhancement factors to assess the overall effect of Nu and f. For $\beta_1 = 15°$ and $\beta_2 = 5°$, a significant enhancement in the heat transfer performance was obtained with a moderate pressure drop. In other words, the enhancement factor reaches its maximum in these angular positions of the two winglet pairs for both $Re_H = 611$ and 819.

Table 4 makes a comparison between the maximum overall thermo-fluid performance obtained in the present study and that obtained from some of the recent contributions of different researchers. According to this table, the split winglet pairs supporting the elliptical tube combination enhance the heat transfer performance with a moderate pressure drop penalty. As a result, a greater value of η can be obtained using the proposed winglet and tube combination. The table also shows a higher value of η when using VGs with holes [38]. It is expected that the thermo-fluid performance of the proposed split winglet configuration can be further improved by making some holes on the winglet surface.

4. Conclusion

The present investigation attempted to analyze the thermo-fluid performance of a FTHX with the rectangular winglets placed with a heretofore-unused combination-split winglet pairs over the elliptical tubes. The findings of the numerical investigation revealed that the split winglet pairs placed at optimum attack angles would compress the wake region of the winglet supported tube as well as the adjacent tube, thus resulting in significant heat transfer enhancement. In addition, the impacts of the stream- and span-wise locations of the split winglet pair were also investigated. Some of major conclusions drawn from the present study are summarized below:

- The FTHX with an elliptical tube configuration exhibited greater overall thermo-fluid performance than that with a circular tube configuration due to its significantly low pressure drop.
- Based on the highest enhancement factor, the optimum stream- and span-wise locations were obtained at ΔX_1= -2.67 mm, ΔX_2 = +2.67 mm, ΔY_1 = 9 mm, and ΔY_2 = 7 mm, respectively, for the split winglet pairs where the enhancement factor increased to 13–15%.
- The attack angles of the front and rear winglet pairs were found to have a great impact on the overall thermo-fluid performance of the FTHX. For both Re_H = 611 and 819, the enhancement factor was found at its maximum value (about 15-16% higher than that of the baseline model) when the front and rear winglets were set to the attack angles of 15° and 5°, respectively.

The thermo-fluid performance of the circular tube geometry was expected to be higher than that of the elliptical tube configurations at larger Reynolds numbers ($Re_H > 900$). Therefore, the results given in the present numerical investigation on the elliptical tubes with split winglet pairs were limited to applications involving flows with low velocity ($Re_H <$ 900). Moreover, in the present work, computations were performed considering the in-line arrangement of tubes. Similar computations can also be performed for the staggered arrangement of tubes to make a better comparison in terms of produced cooling effect and pressure drop penalty.

Acknowledgment

The computations for the present research work were performed at BIT Mesra, Ranchi. The authors are grateful for the institutional supports in the form of computational and library facility.

Nomenclature

$A_{\min}$	Minimum free flow area (m^2)
A_T	Total heat transfer surface area (m^2)
a	Length of semi-minor axis (m)
b	Length of semi-major axis (m)
C	Specific heat of aluminum (J/kg K)
C_P	Specific heat of air (J/kg K)
D	Tube diameter (m)
f	Friction factor (m)
F_t	Fin thickness (m)
FTHX	Fin-and-tube heat exchanger
h	Heat transfer coefficient (W/m^2K)
H	Fin spacing (m)
k	Thermal conductivity (W/m K)
L	Flow length (m)
L_1	Front winglet length (m)
L_2	Rear winglet length (m)
$\dot{m}$	Mass flow rate (kg/s)
n	Number of tube rows
Nu	Nusselt number
P	Pressure (Pa)
Pa	Atmospheric pressure (Pa)
Pl	Longitudinal tube pitch (m)
Pt	Transverse tube pitch (m)
ΔP	Pressure drop (Pa)
$\overline{p}$	Total average pressure (Pa)
Q	Heat transfer capacity (W)
Re	Reynolds number
Re_D	Reynolds number based on tube diameter
Re_{Dh}	Reynolds number based on hydraulic diameter
Re_H	Reynolds number based on channel height
T	Temperature (K)
ΔT	Log mean temperature difference (K)
$\overline{T}$	Total average temperature (K)
u	Velocity in x-direction (m/s)
v	Velocity in y-direction (m/s)
VG	Vortex Generator
w	Velocity in z-direction (m/s)
ΔX	stream wise eccentric separation (m)
ΔX_1	Stream wise position for front winglet (m)
ΔX_2	Stream wise position for rear winglet (m)
ΔY	stream wise eccentric separation (m)
ΔY_1	Span wise position for front winglet (m)
ΔY_2	Span wise position for rear winglet (m)

Subscripts

al	Aluminum
a	Air
c	Circular tube configuration
$down$	Bottom surface of the domain
e	Elliptical tube configuration
in	Inlet parameter
max	Maximum
o	Outlet parameter
0	Smooth channel
up	Top surface of the domain
w	Wall

Greek symbols

α	Thermal diffusivity (m^2/s)
β_1	Angle of attack for front winglet (degree)
β_2	Angle of attack for rear winglet (degree)
η	Enhancement factor
μ	Dynamic viscosity (Pa.s)
ρ	Density of air (kg/m^3)

References

1. Jacobi, A.M. and Shah, R.K. "Heat transfer surface enhancement through the use of longitudinal vortices: A review of recent progress", *Exp. Therm. Fluid Sci.*, **11**(3), pp. 295–309 (1995).

2. Biswas, G., Torii, K., Fujii, D., et al. "Numerical and experimental determination of flow structure and heat transfer effects of longitudinal vortices in a channel flow", *Int. J. Heat Mass Transf.*, **39**(16), pp. 3441–3451 (1996).

3. Torii, K., Kwak, K.M., and Nishino, K. "Heat transfer enhancement accompanying pressure-loss reduction with winglet-type vortex generators for fin-tube heat exchangers", *Int. J. Heat Mass Transf.*, **45**(18), pp. 3795–3801 (2002).

4. Jain, A., Biswas, G., and Maurya, D. "Winglet-type vortex generators with common-flow-up configuration for fin-tube heat exchangers", *Numer. Heat Transf. Part A Appl.*, **43**(2), pp. 201–219 (2003).

5. Jain, A., Biswas, G., and Maurya, D. "Winglet-type vortex generators with common-flow-up configuration for fin-tube heat exchangers", *Numer. Heat Transf. Part A Appl.*, **43**(2), pp. 201–219 (2003).

6. Sohankar, A. and Davidson, L. "Effect of inclined vortex generators on heat transfer enhancement in a three-dimensional channel", *Numer. Heat Transf. Part A Appl.*, **39**, pp. 433–448 (2001).

7. Kwak, K.M., Torii, K., and Nishino, K. "Simultaneous heat transfer enhancement and pressure loss reduction for finned-tube bundles with the first or two transverse rows of built-in winglets", *Exp. Therm. Fluid Sci.*, **29**, pp. 625–632 (2005).

8. Sinha, A., Chattopadhyay, H., Iyengar, A.K., et al. "Enhancement of heat transfer in a fin-tube heat exchanger using rectangular winglet type vortex generators", Int. *J. Heat Mass Transf.*, **101**, pp. 667–681 (2016).

9. Joardar, A. and Jacobi, A.M. "A numerical study of flow and heat transfer enhancement using an array of delta-winglet vortex generators in a fin-and-tube heat exchanger", *J. Heat Transfer*, **129**, p. 1156 (2007).

10. Joardar, A. and Jacobi, A.M. "Heat transfer enhancement by winglet-type vortex generator arrays in compact plain-fin-and-tube heat exchangers", Int. *J. Refrig.*, **31**, pp. 87–97 (2008).

11. He, Y.L., Chu, P., Tao, W.Q., et al. "Analysis of heat transfer and pressure drop for fin-and-tube heat exchangers with rectangular winglet-type vortex generators", *Appl. Therm. Eng.*, **61**, pp. 770–783 (2013).

12. Richter do Nascimento, C.A., Mariani, V.C., and Coelho, L. dos S. "Integrative numerical modeling and thermodynamic optimal design of counter-flow plate-fin heat exchanger applying neural networks", *Int. J. Heat Mass Transf.*, **159**, p. 120097 (2020).

13. Galuzio, P.P., de Vasconcelos Segundo, E.H., dos Santos Coelho, L., et al. "MOBOpt - multi-objective Bayesian optimization", *Software X*, **12**, p. 100520 (2020).

14. Vasconcelos Segundo, E.H.d., Mariani, V.C., and Coelho, L.d.S. "Metaheuristic inspired on owls behavior applied to heat exchangers design", *Therm. Sci. Eng. Prog.*, **14**(January), p. 100431 (2019).

15. Lemouedda, A., Breuer, M., Franz, E., et al. "Optimization of the angle of attack of delta-winglet vortex generators in a plate-fin-and-tube heat exchanger", *Int. J. Heat Mass Transf.*, **53**, pp. 5386–5399 (2010).

16. Salviano, L.O., Dezan, D.J. and Yanagihara, J.I. "Optimization of winglet-type vortex generator positions and angles in plate-fin compact heat exchanger: Response surface methodology and direct optimization", Int. *J. Heat Mass Transf.*, **82**, pp. 373–387 (2015).

17. Venegas, T., Qu, M., Nawaz, K., et al. "Critical review and future prospects for desiccant coated heat exchangers: Materials, design, and manufacturing", *Renew. Sustain. Energy Rev.*, **151**, p. 111531 (2021).

18. Wajs, J., Kura, T., Mikielewicz, D., et al. "Numerical analysis of high temperature minichannel heat exchanger for recuperative microturbine system", *Energy*, **238**, pp. 121683 (2022).

19. Tian, L., He, Y., Chu, P., et al. "Numerical study of flow and heat transfer enhancement by using delta winglets in a triangular wavy fin-and-tube heat exchanger", *J. Heat Transfer*, **131**, pp. 091901 (2009).

20. Saha, P., Biswas, G., and Sarkar, S. "Comparison of winglet-type vortex generators periodically deployed in a plate-fin heat exchanger-A synergy based analysis", *Int. J. Heat Mass Transf.*, **74**, pp. 292–305 (2014).

21. Sinha, A., Raman, K.A., Chattopadhyay, H., et al. "International journal of heat and mass transfer effects of different orientations of winglet arrays on the performance of plate-fin heat exchangers", *Int. J. Heat Mass Transf.*, **57**, pp. 202–214 (2013).

22. Gentry, M.C. and Jacobi, A.M. "Heat transfer enhancement by delta-wing vortex generators on a flat plate: Vortex interactions with the boundary layer", *Exp. Therm. Fluid Sci.*, **14**, pp. 231–242 (1997).

23. Gentry, M.C. and Jacobi, A.M. "Heat transfer enhancement by delta-wing-generated tip vortices in flat-plate and developing channel flows", *J. Heat Transfer*, **124**, pp. 1158–1168 (2002).

24. Pesteei, S.M., Subbarao, P.M.V. and Agarwal, R.S. "Experimental study of the effect of winglet location on heat transfer enhancement and pressure drop in fin-tube heat exchangers", *Appl. Therm. Eng.*, **25**, pp. 1684–1696 (2005).

25. Arora, A., Subbarao, P.M.V. and Agarwal, R.S. "Numerical optimization of location of 'common flow up' delta winglets for inline aligned finned tube heat exchanger", *Appl. Therm. Eng.*, **82**, pp. 329–340 (2015).

26. Sarangi, S.K. and Mishra, D.P. "Effect of winglet location on heat transfer of a fin-and-tube heat exchanger", *Appl. Therm. Eng.*, **116**, pp. 528–540 (2017).

27. Sarangi, S.K., Mishra, D.P. and Mishra, P. "Numerical analysis of thermofluid performance of fin-and-tube heat transfer surface using rectangular winglets", *J. Heat Transfer*, **141**, p. 101801 (2019).

28. Sarangi, S.K., Mishra, D.P., and Mishra, P. "Parametric investigation of wavy rectangular winglets for heat Transfer enhancement in a fin-and-tube heat transfer surface", *J. Appl. Fluid Mech.*, **13**, pp. 615–628 (2020).

29. Naik, H. and Tiwari, S. "Effect of winglet location on performance of fin-tube heat exchangers with inline tube arrangement", *Int. J. Heat Mass Transf.*, **125**, pp. 248–261 (2018).

30. Deepakkumar, R. and Jayavel, S. "Air side performance of finned-tube heat exchanger with combination of circular and elliptical tubes", *Appl. Therm. Eng.*, **119**, pp. 360–372 (2017).

31. Richter do Nascimento, C., Cocco Mariani, V., and dos Santos Coelho, L. "Experimental analysis of R410A flow in helically rib-roughened tubes", *Therm. Sci. Eng. Prog.*, **20**(June), p. 100668 (2020).

32. Caliskan, S. "International journal of heat and mass transfer experimental investigation of heat transfer in a channel with new winglet-type vortex generators", *Int. J. Heat Mass Transf.*, **78**, pp. 604–614 (2014).

33. Kays, W.M. and London, A.L., *Compact Heat Exchangers*, 3rd Ed., pp. 270–271, McGraw-Hill, New York (1998).

34. Gholami, A.A., Wahid, M.A., and Mohammed, H.A. "Heat transfer enhancement and pressure drop for fin-and-tube compact heat exchangers with wavy rectangular winglet-type vortex generators", *Int. Commun. Heat Mass Transf.*, **54**, pp. 132–140 (2014).

35. Gholami, A., Wahid, M.A., and Mohammed, H.A. "Thermal-hydraulic performance of fin-and-oval tube compact heat exchangers with innovative design of corrugated fin patterns", *Int. J. Heat Mass Transf.*, **106**, pp. 573–592 (2017).

36. Qian, Z., Wang, Q., and Cheng, J. "Analysis of heat and resistance performance of plate fin-and-tube heat exchanger with rectangle-winglet vortex generator", *Int. J. Heat Mass Transf.*, **124**, pp. 1198–1211 (2018).

37. Naik, H. and Tiwari, S. "Thermal performance analysis of fin-tube heat exchanger with staggered tube arrangement in presence of rectangular winglet pairs", *Int. J. Therm. Sci.*, **161**, p. 106723 (2021).

38. Modi, A.J., Kalel, N.A., and Rathod, M.K. "Thermal performance augmentation of fin-and-tube heat exchanger using rectangular winglet vortex generators having circular punched holes", *Int. J. Heat Mass Transf.*, **158**, pp. 1–16 (2020).

39. Khan, T.A. and Li, W. "Optimal configuration of vortex generator for heat transfer enhancement in a plate-fin channel", *J. Therm. Sci. Eng. Appl.*, **10**(2), p. 021013 (2017).

Biographies

Shailesh Kumar Sarangi received his PhD from Birla Institute of Technology, Mesra, India in 2021. His research interest includes heat transfer enhancement in heat exchangers using passive enhancement methods. He received his ME degree in Mechanical Engineering from Birla Institute of Technology, Mesra in 2016. In his Master's dissertation, he evaluated the thermo-fluid performance of fin-and-tube heat exchangers and graduated with an excellent grade from the university.

Dipti Prasad Mishra is a Professor of Mechanical Engineering at Birla Institute of Technology, Mesra, Ranchi, India. He received his BE and ME degrees in Engineering from VSSUT, Burla, Odisha, India. He obtained his PhD in Mechanical Engineering at the IIT Kharagpur, India in 2009 . He is currently working in the field of computational fluid dynamics and heat transfer. He has authored many international publications in CFD and heat transfer area.